Nuclear Instruments and Methods in Physics Research A 788 (2015) 73–78

Contents lists available at ScienceDirect

Nuclear Instruments and Methods in Physics Research A

journal homepage: www.elsevier.com/locate/nima

Monte Carlo simulation of a fast neutron counter for use in neutron radiography

Mohsen Meshkian

Department of Mechanical and Process Engineering, ETH Zurich, 8092 Zurich, Switzerland

ARTICLE INFO

Article history:
Received 20 January 2015
Received in revised form
8 March 2015
Accepted 16 March 2015
Available online 25 March 2015

Keywords:
Geant4
Moderator
ZnS(Ag) scintillator
Fast neutron detector
Radiography

ABSTRACT

In this paper, a Geant4 Monte Carlo simulation is employed to evaluate the response of a neutron detection sheet composed of a layer of plexiglas as neutron-to-proton converter and a layer of silver-activated zinc sulphide (ZnS(Ag)) as phosphor. ZnS(Ag) scintillators have the largest light output among the scintillators for fast-neutron spectroscopy. The simulations are performed for ^{252}Cf neutrons which after impinging the converter layer of the detector produce recoil protons. Recoil protons that interact with the scintillator deposit energy which is converted to scintillation light. In this report, different aspects of the ZnS(Ag)-detector, such as the effective converter and scintillator thickness, as well as the detector response are investigated.

1. Introduction

Over the last decade there has been considerable interest in exploring the use of neutron-based techniques for non-destructive screening and elemental characterization of bulk materials. Typically the absorption of X-rays is proportional to the electron density of the investigated subject, while the absorption of thermal neutrons varies rapidly from isotope to isotope, enabling quite distinct imaging modalities compared to photon based techniques. Fast neutrons have unique material penetration properties since the total macroscopic cross-section for fast neutrons is less than its thermal-neutron counterpart, thus enabling a larger penetration depth. For the same reason, fast neutron emissions are much more difficult to shield properly and are suited for the detection of special nuclear materials (SNMs). Another advantage of fast-neutron radiography is the use of resonant features of the scattering cross-sections: the total microscopic cross-section of most isotopes is strongly dependent on the neutron energy. By selecting neutrons within a certain energy range, it is possible to enhance or reduce the contrast between different materials in the object. Finally, fast neutron radiation is more specific than other type of ionizing radiations since it has a lower natural background compared to gamma, beta and alpha emissions.

The aim of this report is to introduce the development of a new fast-neutron detection system used for radiography and spectroscopy measurements. To our knowledge there have been no works dealing with fast-neutron radiography by using separate converter and scintillating material. All the works found [1–5] concerns ZnS (Ag) suspended in an organic material.

2. Detection mechanism

The neutron lacks an electric charge and therefore will only be detected indirectly after interaction with an appropriate converter material on top of the detector [6–11]. The cross-section of the neutron depends strongly on the neutron energy and the target nucleus, which makes the choice of the converter material crucial [12].

Hydrocarbons are potentially good detector media for fast neutrons because they have the highest hydrogen content of all available materials. In the current work, plexiglas is employed as the converter material because of the transparency which becomes important in a future multilayer version of the detector. The simulated detector is shown in Fig. 1 with the essential parts labeled. Fast neutrons crossing the converter (plexiglas) produce secondary protons through elastic interaction with the converter material. These secondary charged particles will interact with the scintillator, which is attached to the converter layer, mostly through electrostatic attractions, ionizing the matter that they pass through and depositing their energy by transferring energy to the kinetic energy of electrons. The released electrons are then converted into light by ionizing the scintillation medium. The produced scintillation light is afterwards collected by a PMT and subsequently transformed into an electrical signal.

E-mail address: mohsen.meshkian@psi.ch

http://dx.doi.org/10.1016/j.nima.2015.03.048
0168-9002/

2.1. Deposition energy

The basic mechanism for slowing down of a charged particle in motion is Coulombic interactions between the particle and electrons in the medium. A charged particle passing through a medium loses energy primarily through the ionization and excitation of atoms. Electromagnetic forces are exerted by the moving charged particle on atomic electrons and energy is imparted to these electrons. If the energy is sufficient an electron of an atom will be knocked out and thus ionized, or the charged particle may leave the atom in an excited, non-ionized state.

Fig. 2 depicts the relation between the incoming recoil proton energy and its deposition energy inside the active volume of the detector using Geant4 [13]. From the figures, it is obvious that a maximum energy is transferred from the proton to the scintillator before it leaves the scintillator. Fig. 2a–c shows that the thickness of the scintillator is not sufficient to stop the incoming recoil proton, thus after a maximum value in the deposition energy (corresponding to the maximum energy transfer) the proton escapes the scintillator. Only scintillators with thicknesses above 400 μm stop the recoil protons. In further, the decreasing effect in the deposition energy is a result of an increased range of the proton (larger than the scintillator thickness) as its kinetic energy increases.

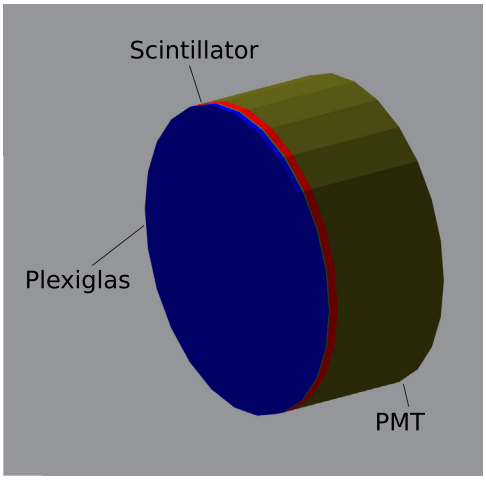

Fig. 1. A schematic over the simulated fast-neutron detector.

3. Neutron source

3.1. ^{252}Cf

^{252}Cf ($T_{1/2} = 2.645$ years) is an artificial radioisotope which is used extensively in research, industry, and medicine as a portable neutron source. The average number of neutrons emitted is about 3.753 ± 0.01 per fission, therefore 1 mg of ^{252}Cf generates 2.314×10^9 neutrons/s with a specific activity of 0.536 mCi/μg [14]. ^{252}Cf decay 96.91% of time through alpha emission and 3.09% of time by spontaneous fission. The neutron spectrum is similar to a fission spectrum, with the most probable energy of 0.7 MeV and an average energy of 2.1 MeV (see Fig. 3). In addition to neutron and alpha emissions, this source also radiates γ-rays. The ratio of the gammas to the neutrons is $N_\gamma/N_n \approx 2.13$; where $N_\gamma \sim 8$ and $N_n \sim 3.75$ are the experimental mean multiplicity values per fission event [15].

A set of measurement with a NaI(Tl) was performed to determine the γ-ray spectrum of the source. The measurement result is shown in Fig. 4. As illustrated, most of the emitted γ-ray energy is in the lower part of the spectrum. The maximum detected energy is about 1.4 MeV.

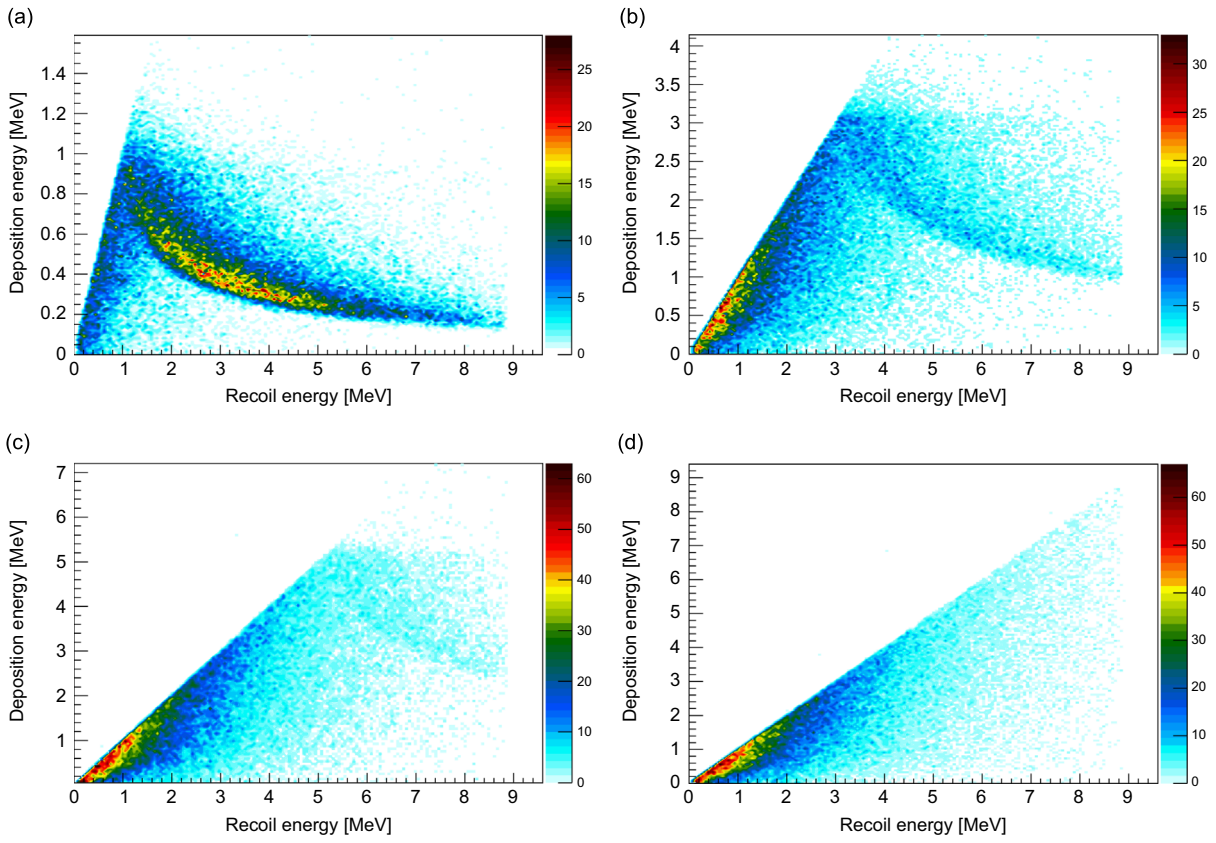

Fig. 2. Deposition energy as a function of recoil proton energy inside the scintillator material with different thicknesses. (a) 10 μm, (b) 65 μm, (c) 150 μm, and (d) 400 μm.

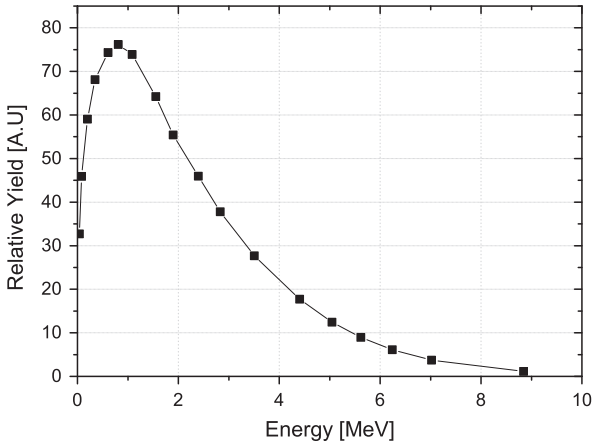

Fig. 3. ^{252}Cf neutron spectrum [16].

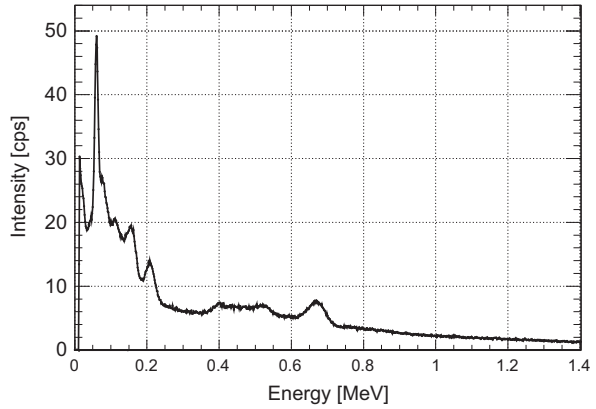

Fig. 4. ^{252}Cf gamma spectrum measured with a NaI(Tl) detector.

Consequently, the maximum deposition energy in the ZnS(Ag) is about 1.4 MeV, although most of the deposited energy will be much lower.

4. Geant4 simulation

4.1. Introduction

Geant4 [13] (GEometry And Tracking) package is a toolkit, utilized for simulation of the passage of particles through matter. It consists of a range of functionalities, such as geometry, physics, primary beam generation, tracking, sensitive detectors, and hits. Geant4 provides the user the basic tools for development of basic and advanced simulation applications in high energy physics, nuclear physics, astrophysics and medical physics.

In this study, a Geant4 Monte Carlo code has been developed for the simulation of the γ-ray and neutron interactions in the detector. All relevant physical processes for γ-rays and neutrons in the energy range in question were included in the simulation. For γ-ray interactions, the data file G4EMLOW version 6.32, containing cross-sections for low energy electromagnetic processes, is used. For neutrons, the data file G4NDL version 4.2 is used. It contains cross-section data compiled from a large number of evaluated neutron reaction data libraries (see Ref. [13]).

The relevant physical processes for detection of fast neutrons in the detector include interaction of the incident fast neutron with the plexiglas, the emission of the secondary proton with the correct energy spectrum, its passage through the converter layer into the scintillator, and finally the deposition energy inside the scintillator. Relevant physical processes for the γ-rays include the interaction with the scintillator through three possible reactions, namely Compton scattering, photoelectric effect, and pair-production. In these processes, secondary electrons are produced which excite the atoms in the scintillator, releasing visible light.

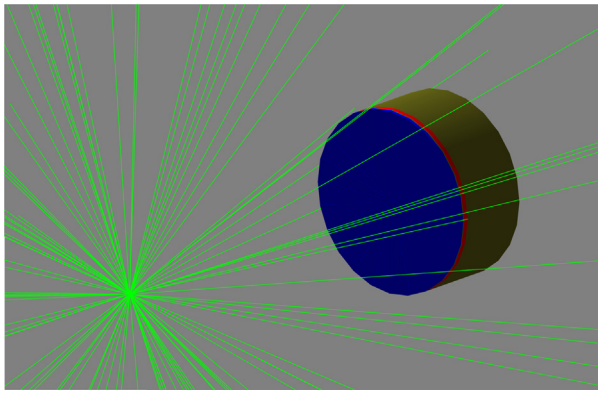

Fig. 5. The source–detector assembly in Geant4. The source-to-detector distance is 10 cm.

4.2. Geometry

The geometry of the experimental setup is implemented with several simplifications. The cavity of the detector consisting of the HV-base and the μ-methal around the PMT were not included in the simulation. The table, which the detector rested on, the floor and the nearby wall and all other equipments in the room were not included in the simulation. The simulated detector, consisting of a plexiglas, a scintillator and a PMT, is depicted in Fig. 5. The ^{252}Cf radionuclide source is assumed as a point source of fast neutrons. It irradiates fast neutrons in 4π with the energy distribution given by Fig. 3.

4.3. Detector response

The optimum converter thickness is the thickness for which the highest number of recoil protons escape the foil – the conversion efficiency increases with the converter thickness and saturates at a value corresponding to the range of the most energetic recoil proton in plexiglas. All the protons created at distances larger than the aforementioned range, cannot escape the foil. An optimum thickness of the plexiglas is one of the important parameters in detector design. The rate of the elastic recoil increases with the converter thickness and consequently, more protons are produced. On the other hand, if the thickness gets close to the range of the protons in plexiglas, some of the recoil protons are stopped before entering the scintillator medium.

5. Simulation results

In the present simulation study, fast-neutron sensitivity of the converter, as well as the recoil proton energy distribution in the scintillator have been investigated.

To find the best achievable detection efficiency it is necessary to first examine the proton range in plexiglas. The projected range, calculated using the SRIM code [17], is shown in Fig. 6. As an example, the protons with highest energy of about 10 MeV have a range inside plexiglas of about 1.0 mm. Accordingly, the maximum detection efficiency of 10 MeV neutrons is limited to a plexiglas converter of 1.0 mm thickness.

The results from Geant4 simulations show that an increase of converter layer thickness increases the (n,p) reaction rate and consequently the number of recoil protons in the converter. Some of the

protons are stopped as they are transported through plexiglas and consequently, the integral flux density of recoil protons reaching the active volume of the detector reaches its maximum for a specific converter layer thickness. The energy distribution of the protons reaching the active volume of the detector after passing the plexiglas is depicted in Fig. 7. The proton flux as well as all other calculated quantities is normalized with the number of neutrons emitted by the source (s.n. in the figures stands for source neutrons). The proton deposition energy inside the scintillator increases as the converter layer thickness increases.

The detection efficiency, i.e. the ratio of the number of protons exiting the converter layer (entering the active volume) to the number of incident neutrons on the converter layer, calculated for different converter layer thicknesses for different incident neutron energies is plotted in Fig. 8. In these graphs, one can follow the tendency of both proton flux density and detection efficiency to grow with increasing converter thickness until 1 mm, followed by reduction of detection efficiency with further increase of converter layer thickness.

The optimum thickness of the converter layer is derived from the dependency of the detection efficiency on the converter layer thickness. According to the Geant4 calculations, the highest detection efficiency is about 0.046% for a converter layer thickness of 1 mm.

In further, the average energy deposited by recoil protons in the active volume of the detector based on ZnS(Ag) is calculated and its dependency on the active thickness is depicted. The results are presented in Fig. 9. As shown, the deposition energy saturates for an active volume of about 400 μm. In thinner active volumes, the protons do not deposit all their energies and consequently, the signal to noise ratio decreases.

Fig. 10 illustrates the energy distribution of pulses created in the active volume of the detector. The energy distributions of the pulses were calculated for different thicknesses of the active volume, namely from 10 to 250 μm. In this case, only the energy deposited by recoil protons was assumed. As shown in the figure, the shape of the proton spectrum agrees with that of the incident proton flux density for the active volume thickness of at least 250 μm.

5.1. Deposition energy

As a first approach, the author has divided the ^{252}Cf spontaneous fission source into one neutron source with the spectrum given in Fig. 3 and the gamma spectrum shown in Fig. 4. In this procedure, the detector was irradiated with each of the sources separately. Fig. 11 depicts the detector configurations that were examined, both with simulations and experiments.

Fig. 12 illustrates the energy spectrum of γ-rays and fission neutrons inside a 65 μm thick ZnS(Ag), normalized to the number of incoming particles and the detector surface area per second. The graph also depicts the superposition of the two distributions. The graph illustrates that the γ-rays deposit energy up to a maximum of 900 keV (see Fig. 12), and that most of the recoil electrons are in the lower keV energy range. On the other hand, fast neutrons

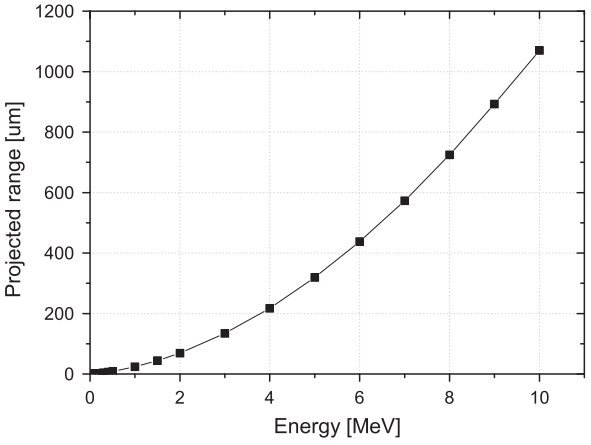

Fig. 6. Proton projected range in plexiglas calculated by SRIM.

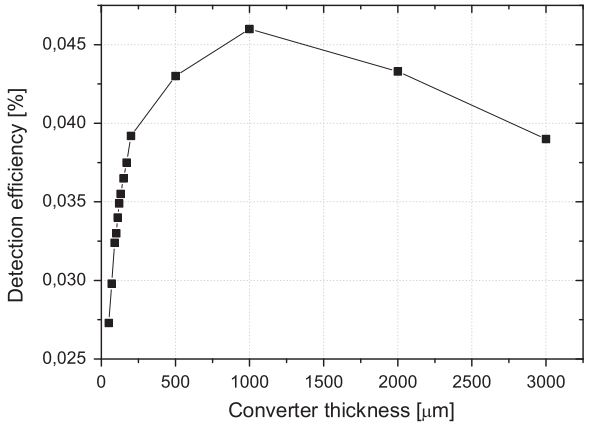

Fig. 8. Calculated detection efficiency of fast-neutron detection for ^{252}Cf neutron source.

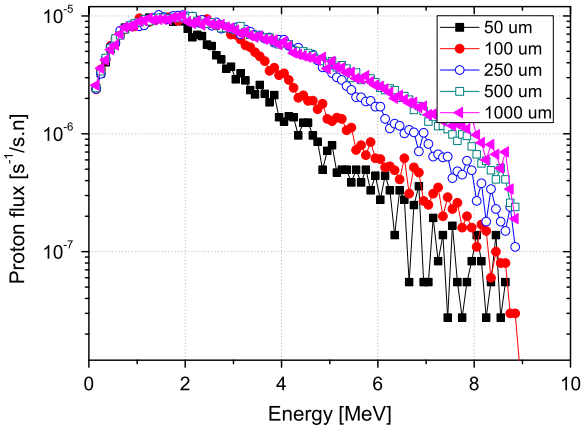

Fig. 7. Deposition energy of recoil protons inside the active region for different converter layer thicknesses.

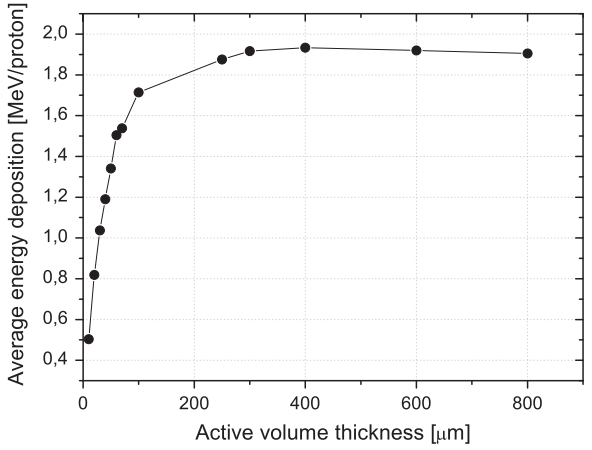

Fig. 9. Proton deposition energy averaged over an active volume of ZnS(Ag).

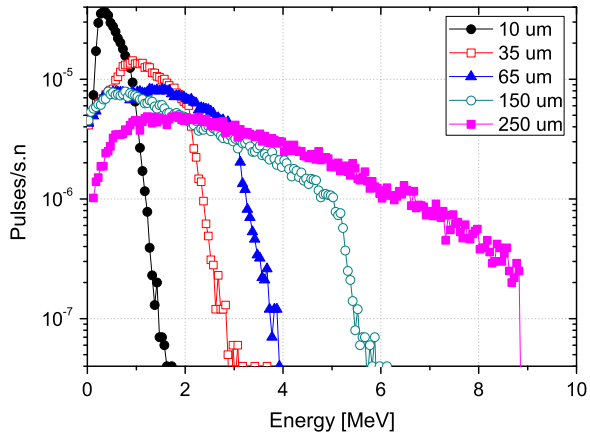

Fig. 10. Deposition energy of recoil protons in the detector calculated for different thicknesses of the active volume. The optimum thickness of the converter layer of 1 mm is assumed.

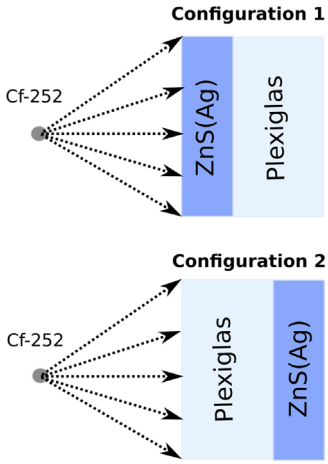

Fig. 11. Detector configurations used both for the Monte Carlo simulations and experiments. The dimensions shown in the figure are not actual.

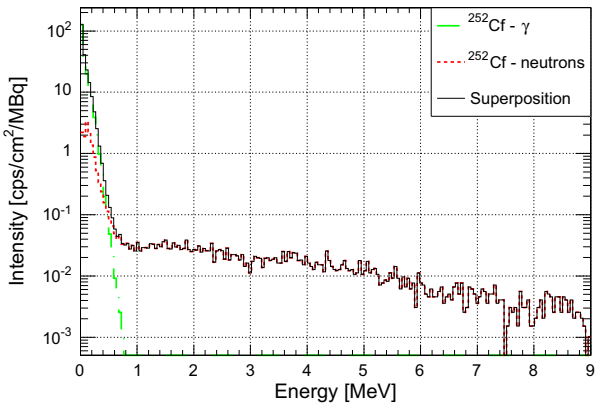

Fig. 12. Energy spectrum of ^{252}Cf source, simulated for Configuration 1. Superposition of the two spectra is also plotted.

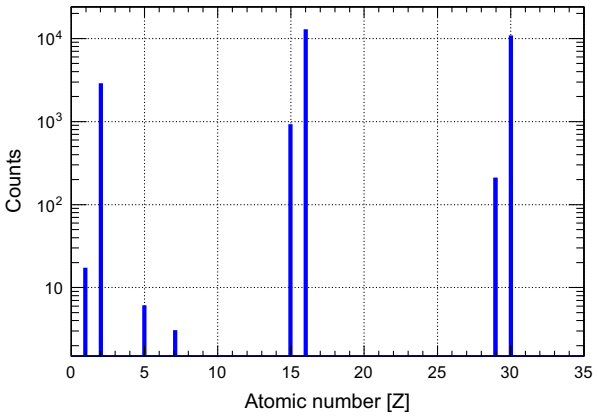

Fig. 13. Secondary nuclei produced by interaction of fast neutrons with the detector material, i.e. the converter layer and the scintillator. Here, production of recoil protons through the direct fast-neutron interaction with the converter layer is neglected.

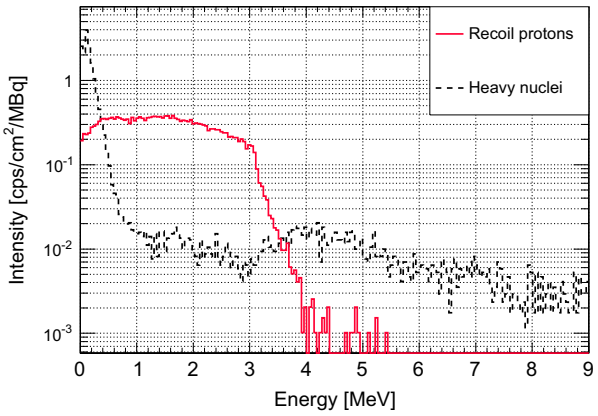

Fig. 14. Energy spectrum of neutron-induced particles, simulated for Configuration 2.

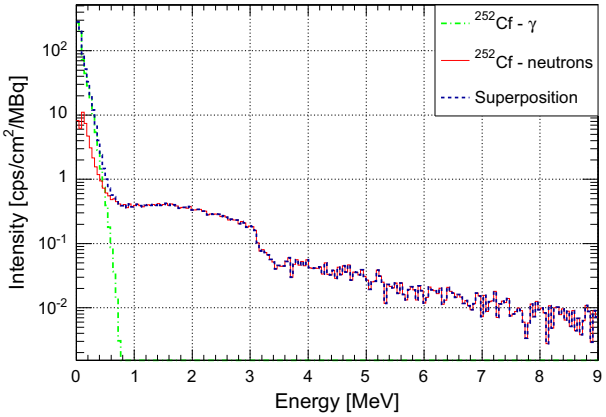

Fig. 15. Energy spectrum of ^{252}Cf source, simulated for Configuration 2. Superposition of the two spectra is also plotted.

create recoil protons with energies from 0 up to the energy of the incoming neutron. The energy deposition spectrum of recoil protons is proportional to that of their kinetic energy.

For Configuration 2, the neutrons are first transported through the converter layer (plexiglas). The emitted recoil protons deposit energy inside the active volume, together with other residuals produced by fast-neutron interaction in the whole detector volume. Fig. 13 illustrates the residuals produced in the detector volume, i.e. the converter layer and the scintillator. From the figure one could recognize the recoil nuclei of S ($Z=16$) and Zn ($Z=30$), from the interaction of the scintillator material with fast neutrons. The energy spectrum in the scintillator, produced by residuals from the fast-neutron interaction with the converter layer and the scintillator, is depicted in Fig. 14. The solid spectrum illustrates the energy spectrum of recoil protons produced in the converter layer. The dashed spectrum illustrates all other particles which are

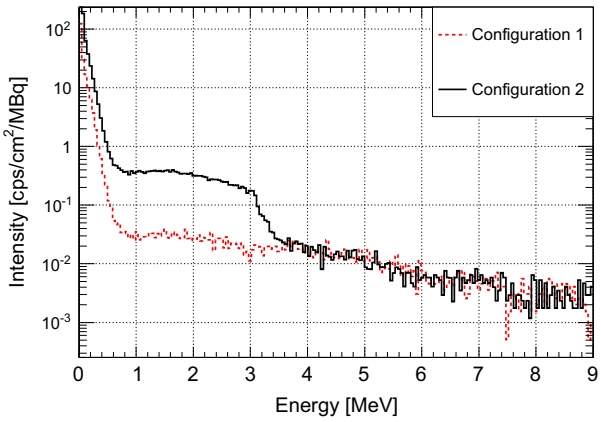

Fig. 16. Energy spectrum comparison between Configurations 1 and 2.

produced in the converter layer and the scintillator that deposit their energy inside the scintillator.

Fig. 15 depicts the energy spectrum inside the active region of the detector as a superposition of energy spectrum of γ-rays and that of the residuals produced by fast neutrons. As illustrated, the γ-rays contribute only to energies up to 900 keV. The larger part of the spectrum corresponds to the deposition energy of fast neutrons.

Furthermore, it is important to compare the energy spectra of neutrons and gamma particles for both of the configurations. Fig. 16 illustrates the difference between the two spectra. As depicted in the figure, Configuration 2 results in a larger efficiency inside the scintillator which is due to the energy of the recoil protons exiting the converter layer.

6. Conclusions and outlook

In this paper, a Monte Carlo simulation has been developed for analyzing the performance of ZnS(Ag) scintillators when attached to an organic converter layer for fast-neutron detection. The optimum thickness of the converter layer was calculated to 1 mm and that of the scintillator was calculated to 400 μm. But this is very thick for the scintillator to transmit its own light effectively.

The total light output of the scintillator per incident neutron is the product of the average number of escaped neutron-to-proton interactions in the converter, and the average amount of energy deposited in the scintillator by recoil protons and other heavy nuclei created in the detector. The first factor depends on the effective thickness of the converter, and the second one depends on the thickness of the scintillator.

These detectors are used to detect recoil protons produced by neutrons, mostly by (n,p)-scattering in the converter layers. The advantage of a separate scintillator is the neutron-insensitivity of the scintillator which can be useful for energy-selectivity applications. This advantage is common for all inorganic scintillators. Another advantage of ZnS(Ag) scintillator is its γ insensitivity. This is due to the fact that it can be made very thin for which the γ-interaction probability decreases.

A new detector system is under development which uses a multilayer version of the detector presented in this work. One of the features of this new system is the higher detection efficiency it has compared to its monolayer counterpart.

References

[1] K. Yoshii, K. Miya, Nuclear Instruments and Methods in Physics Research A 346 (1994) 253.
[2] H. Rahmanian, J. Watterson, Nuclear Instruments and Methods in Physics Research B 139 (1998) 466.
[3] B. Tang, et al., Nuclear Instruments and Methods in Physics Research A 729 (2013) 327.
[4] V.I. Mikerov, et al., Applied Radiation and Isotopes 61 (2004) 529.
[5] G. Chen, Fast neutron resonance radiography for elemental imaging: theory and applications, Department of Nuclear Engineering, Massachusetts Institute of Technology, 2001, (Ph.D. thesis).
[6] A. Sagatova-Perdochova, et al., Nuclear Instruments and Methods in Physics Research A 591 (2008) 98.
[7] K. Sedlackova, et al., Nuclear Instruments and Methods in Physics Research A 709 (2013) 63.
[8] J. Uher, et al., Nuclear Instruments and Methods in Physics Research A 591 (2008) 71.
[9] M. Ladziansky, et al., Nuclear Instruments and Methods in Physics Research A 607 (2009) 135.
[10] J. Jakubek, et al., Nuclear Instruments and Methods in Physics Research A 569 (2006) 205.
[11] J. Bouchami, et al., Nuclear Instruments and Methods in Physics Research A 633 (2011) S226.
[12] M. Abbrescia, et al., Nuclear Instruments and Methods in Physics Research A 533 (2004) 149.
[13] S. Agostinelli, et al., Nuclear Instruments and Methods in Physics Research A 506 (2003) 250.
[14] R. Martin, et al., Journal of Radioanalytical and Nuclear Chemistry 236 (2008) 5.
[15] M. Palomba, G. Erasmo, A. Pantaleo, Nuclear Instruments and Methods in Physics Research A 498 (2003) 384.
[16] A. Smith, P. Fields, J. Roberts, Physical Review 108 (1957) 411.
[17] J. Ziegler, ⟨http://www.srim.org/⟩.